Accepted Manuscript

Structural, magnetic and vibrational properties of multiferroic $GaFeO_3$ at high pressure

N.O. Golosova, D.P. Kozlenko, S.E. Kichanov, E.V. Lukin, L.S. Dubrovinsky, A.I. Mammadov, R.Z. Mehdiyeva, S.H. Jabarov, H.-P. Liermann, K.V. Glazyrin, T.N. Dang, V.G. Smotrakov, V.V. Eremkin, B.N. Savenko

PII: S0925-8388(16)31335-4

DOI: 10.1016/j.jallcom.2016.04.316

Reference: JALCOM 37535

To appear in: *Journal of Alloys and Compounds*

Received Date: 10 March 2016

Revised Date: 26 April 2016

Accepted Date: 27 April 2016

Please cite this article as: N.O. Golosova, D.P. Kozlenko, S.E. Kichanov, E.V. Lukin, L.S. Dubrovinsky, A.I. Mammadov, R.Z. Mehdiyeva, S.H. Jabarov, H.-P. Liermann, K.V. Glazyrin, T.N. Dang, V.G. Smotrakov, V.V. Eremkin, B.N. Savenko, Structural, magnetic and vibrational properties of multiferroic $GaFeO_3$ at high pressure, *Journal of Alloys and Compounds* (2016), doi: 10.1016/j.jallcom.2016.04.316.

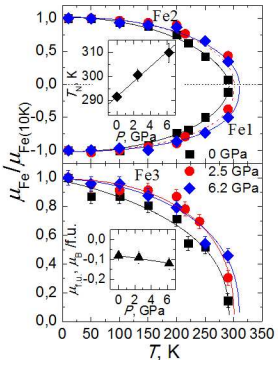

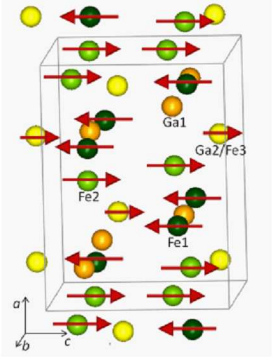

Structural, magnetic and vibrational properties of multiferroic $GaFeO_3$ at high pressure

N.O. Golosova[1*], D.P. Kozlenko[1], S.E. Kichanov[1], E.V. Lukin[1], L.S. Dubrovinsky[2], A.I. Mammadov[3], R.Z. Mehdiyeva[3], S.H. Jabarov[3], H.-P. Liermann[4], K.V. Glazyrin[4], T.N. Dang[5], V.G. Smotrakov[6], V.V. Eremkin[6], and B.N. Savenko[1]

[1] Frank Laboratory of Neutron Physics, Joint Institute for Nuclear Research, 141980 Dubna, Russia

[2] Bayerisches Geoinstitut, Universität Bayreuth, D-95440 Bayreuth, Germany

[3] Laboratory of Non-Standard Control and Diagnostics, Institute of Physics, ANAS, AZ-1143, Baku, Azerbaijan

[4] Photon Sciences, Deutsches Elektronen Synchrotron, D-22607 Hamburg, Germany

[5] Institute of Research and Development, Duy Tan University, 550000 Da Nang,Viet Nam

[6] Physics Research Institute, Southern Federal University, 344090, Rostov-on-Don, Russia

Corresponding Author

**Email address*: golosova@nf.jinr.ru (N.O. Golosova).

Abstract

The crystal, magnetic structure and vibrational spectra of multiferroic $GaFeO_3$ have been studied by means of neutron, X-ray powder diffraction and Raman spectroscopy at pressures up to 6.2 and 42 GPa, respectively. A presence of Fe/Ga antisite disorder leads to a formation of the ferrimagnetic ground state with the Néel temperature T_N = 292 K at ambient pressure. Upon compression, the magnetic ground state symmetry remains the same and the Néel temperature increases with a pressure coefficient $(1/T_N)(dT_N/dP)$ = 0.011(1) GPa^{-1}. Application of high pressure above 21 GPa leads to a gradual structural phase transition from the polar orthorhombic $Pc2_1n$ phase to nonpolar orthorhombic *Pbnm* phase. It is accompanied by anomalies in the pressure behaviour of several Raman modes. Pressure dependencies of lattice parameters and Raman modes frequencies in the observed structural phases were obtained.

PACS: 75.25.-j, 61.50.Ks, 78.30.-j

Keywords: multiferroic, crystal and magnetic structure, x-ray diffraction, neutron diffraction, high pressure, Raman spectroscopy

1. Introduction

Multiferroic materials, demonstrating several ferroic properties, primary magnetism and ferroelectricity in a single phase, attract a great interest due to challenging physical phenomena and wide range of potential applications in multifunctional devices [1-3] (sensors, data storage devices, transducers).

Most of the multiferroic materials can be classified in two types. The first one, conventional multiferroics like $BiFeO_3$ and hexagonal $RMnO_3$ (R – rare earth elements), is characterized by magnetic ordering temperatures significantly lower than the ferroelectric transition ones, resulting in relatively weak magnetoelectric coupling [1, 2]. The second type, found more recently is improper multiferroics, where ferroelectricity is associated with the lattice inversion symmetry breaking by modulated magnetic order. In such materials, which list includes orthorhombic $RMnO_3$, RMn_2O_5 (R = Tb, Ho, Dy, Y and Bi), $RbFe(MoO_4)_2$, the magnetoelectric coupling is much more pronounced and magnetic ordering and ferroelectric transition temperatures are close, but typically much lower ambient temperature, restricting a range of potential technological applications [3-5].

From practical point of view, one of the most attractive multiferroic materials is gallium iron oxides $Ga_{2-x}Fe_xO_3$ ($0.7 \leq x \leq 1.4$). These compounds exhibit a ferrimagnetic order and the magnetic ordering temperature T_N can be tuned in wide limits around ambient temperature (200 - 340 K) depending on chemical composition and synthesis procedure. Their unique magnetoelectric [6], magneto-optic [7] and piezoelectric [8,9] properties are also important for understanding fundamental nature of multiferroicity. At temperatures below T_N $Ga_{2-x}Fe_xO_3$ shows a relatively strong magnetoelectric coupling [9, 10].

One of the most studied representatives of $Ga_{2-x}Fe_xO_3$ family is gallium ferrite $GaFeO_3$. In wide temperature range 4 - 1386 K it exhibits orthorhombic structure of polar $Pc2_1n$ symmetry [11, 12]. It consists of eight formula units per unit-cell with four different cation sites of Ga^{3+} and Fe^{3+}: two sites of Ga^{3+} ions (Ga1 and Ga2), and two sites of Fe^{3+} ions (Fe1 and Fe2). Ga1 is surrounded by oxygen tetrahedron and Ga2 and Fe1 are surrounded by oxygen octahedrons. According to different experiments on x-ray [13] and neutron scattering [11], mössbauer spectroscopy [14] site disorder between Fe/Ga positions was observed in $GaFeO_3$. It becomes possible due to nearly close ionic radii of Fe^{3+} (0.645 Å) and Ga^{3+} (0.62 Å) in octahedral coordination [15]. Antiferromagnetic coupling of magnetic moments of Fe1 and Fe2 atoms was found [11]. The excess of Fe atoms at Ga2 octahedral sites leads to its ferromagnetic

coupling towards to magnetic moments of Fe2 atoms. The magnetization axis is found to be along the *c* axis [11, 16], while the electric polarization - along the *b* axis [11]. First-principles calculations of the total energy [17] for different spin and structural configurations revealed antiferromagnetic spin order in its ground state of ideal crystal structure in multiferroic $GaFeO_3$, which is in agreement with neutron diffraction experiments for stoichiometric $GaFeO_3$ (T_N = 200 K) [11]. Whereas Fe substitution at Ga2 site leads to ferromagnetic arrangement towards to Fe2 [17] and Néel temperature arises. The important factor, seriously affecting magnetic and ferroelectric properties, is the Fe/Ga site disorder, mediating distortions of GaO_6 and FeO_6 polyhedra [11]. It is controlled by the sample preparation method. The inelastic neutron scattering and Raman spectroscopy experiments, as well as first-principles calculations evidence a presence of the strong spin-phonon coupling in $GaFeO_3$ below T_N [18, 19, 14].

Recent high-pressure measurements [20] up to 70 GPa revealed a complex sequence of structural phase transitions in $GaFeO_3$ at compression, decompression and recompression. Upon compression, the perovskite orthorhombic phase (sp. gr. *Pbnm*) was stabilized above 25 GPa with discontinuous volume decrease of about 5.4 %. Further increase of pressure up to 53 GPa caused a reversible isostructural transition, characterized by significant discontinuous drop of the volume of ~ 3%. Decompression experiments showed unexpected first-order structural transition to $LiNbO_3$-type structure (sp. gr. *R*3*c*), which appeared at 24 GPa and remained stable up to ambient pressure. With recompression the stability of the *R*3*c* - phase is preserved up to 50 GPa, above of which it replaced by the *Pbnm* - phase.

Magnetic and electric properties investigations under high pressure [20] revealed a significant changes of T_N and resistance *R* in $GaFeO_3$. As pressure increases up to 33 GPa, an increase of T_N from initial value of 200 K to slightly above room temperature and resistivity drop by one order of magnitude were found. Nevertheless, $GaFeO_3$ remains magnetic insulator up to 56 GPa. In pressure region 62 - 77 GPa a coexistence of insulating clusters of Fe^{3+} moments and conducting nonmagnetic clusters was detected. At P > 77 GPa $GaFeO_3$ becomes nonmagnetic metall. A comparison with the end member of $Ga_{2-x}Fe_xO_3$ family (x = 2), hematite Fe_2O_3 (sp. gr. $R\bar{3}c$) and also $CaFe_2O_4$ (sp. gr. *Pbnm*) showed that the electronic transition to the uncorrelated state occurs at the same pressure (~ 50 GPa) for all investigated ferrites, regardless of the preceding structure, when the relative volume of the FeO_6-polyhedra V_{pol}/V_{0pol} reaches a critical value ~ 0.85 [20]. The observed relationship between electronic and magnetic properties of the high pressure phase of $GaFeO_3$ is consistent with the Mott transition driven by a band-width broadening mechanism [21].

The most of the previous high pressure studies of $GaFeO_3$ were focused on investigations of crystal structure and macroscopic physical properties. Further insight into the relationship between the structural properties and magnetic order of $GaFeO_3$ can be given by the studies of the modifications of the magnetic structure upon variation of structural parameters. In the present paper we report combined x-ray and neutron diffraction, and Raman spectroscopy studies on powder sample $GaFeO_3$ over 0 - 41.8 GPa pressure range and 10 - 300 K temperature range to investigate structure and magnetic moments evolution and the role of phonon excitations across the structural phase transition.

2. Experimental

$GaFeO_3$ powdered sample was obtained from single crystals grown by the flux method [8] using the Ga_2O_3, Fe_2O_3 as sample components and B_2O_3 and Bi_2O_3 as flux components, taken in the weight ratio 12.5:12.5:7.7:67.3.

Angle-dispersive x-ray powder diffraction patterns at high pressures up to 30.5 GPa and ambient temperature were measured at the Extreme Conditions Beamline P02.2 [22] at the third-generation synchrotron radiation source PETRA III located at the Deutsches Elektronen Synchrotron (DESY), Hamburg, Germany. The diffraction images were collected with the wavelength $\lambda = 0.2904$ Å on the amorphous silicon flat panel detector bonded to a ScI scintillator (XRD 1621) from Perkin Elmer and located at a distance of 430.5448 mm from the sample. The two-dimensional x-ray diffraction (XRD) images were converted to one-dimensional diffraction patterns using the FIT2D program [23].

Neutron powder diffraction measurements at high pressures up to 6.2 GPa were performed at selected temperatures in the range of 10–290 K with the DN-12 spectrometer [24] at the IBR-2 high-flux pulsed reactor [Frank Laboratory of Neutron Physics, Joint Institute for Nuclear Research (JINR), Dubna, Russia] using the sapphire anvil high-pressure cell [25]. The pressure was determined by the ruby fluorescence technique [26]. Diffraction patterns were collected at scattering angles 45° and 90°, with the resolution $\Delta d/d = 0.015$. Experimental data of the x-ray and neutron powder diffraction experiments were analyzed by the Rietveld method using the FULLPROF [27].

Raman spectra at ambient temperature and pressures up to 41.8 GPa were collected using a LabRam spectrometer (NeHe excitation laser) with a wavelength of 632.8 nm, 1800 grating, confocal hole of 1100 μm, and x 50 objective. In the X-ray diffraction and Raman experiments,

The BX90 - type diamond anvil cell [28] was used. The sample was loaded into the hole of the 120-μm diameter made in the Re gasket intended to be ~ 30-μm thickness. The diamonds with culets of 250 μm were used. Neon gas loaded under pressure of ~ 0.15 GPa was used as a pressure-transmitting medium. The pressure was determined by the ruby fluorescence technique [26].

3. Results and discussion

3.1. Crystal structure

X-ray diffraction patterns of $GaFeO_3$ at selected pressures and ambient temperature are shown in Fig. 1. In the pressure range 0 - 21.3 GPa they correspond to orthorhombic crystal structure of $Pc2_1n$ symmetry (Fig. 2). The analysis by the Rietveld method has shown that at higher pressures a new phase of orthorhombic crystal structure of *Pbnm* symmetry starts to evolve (Fig. 2). It consists of four formula units per unit-cell with two different cation sites of Ga^{3+} and Fe^{3+}: one site of Ga^{3+} ions and one site of Fe^{3+} ions. Ga ions are eight-fold coordinated and Fe ions are six-fold coordinated. Volume contribution of the new perovskite orthorhombic *Pbnm* - phase reaches 11.5% at 30.5 GPa and the gradual character of the structural transition is consistent with findings by Arielly et al. [20].

Calculated lattice parameters at ambient conditions are in agreement with that one found in previous studies [13, 14, 18, 20]: a = 8.754 (3) Å, b = 9.396(3) Å, c = 5.078 (2) Å.

The obtained pressure dependences of the unit-cell volume and lattice parameters for the $Pc2_1n$-phase of $GaFeO_3$ are shown in Fig. 3. The volume compressibility data were fitted by the Birch-Murnaghan equation of state [29]:

$$P = \frac{3}{2}B_0\left(x^{-\frac{7}{3}} - x^{-\frac{5}{3}}\right)\left[1 + \frac{3}{4}(B' - 4)\left(x^{-\frac{2}{3}} - 1\right)\right],$$

were $x = V/V_0$ is the relative volume change, V_0 is the unit cell volume at P = 0 GPa, and B_0, B' are the bulk modulus [$B_0 = -V(dP/dV)_T$] and its pressure derivative [$B' = (dB_0/dP)_T$]. Calculated value of B_0 = 202.8(2.5) GPa is comparable with one 207 GPa estimated from the Kohn-Sham density functional theory within the local density approximation (LDA) [18] and somewhat less than the value of B_0 = 230(4) GPa, found for stoichiometric $GaFeO_3$ in [20]. The value of the bulk modulus pressure derivative was found to be B' = 4.0(5).

The lattice compression of $GaFeO_3$ is anisotropic. The average compressibility ($k_{ai} = -(1/a_{i0})(da_i/dP)|_T$, $a_i = a, b, c$) of the b – parameter, $k_b = 0.0024$ GPa^{-1}, is about twice larger in comparison with those of the a- and c- parameters, $k_a = 0.0015$ and $k_c = 0.0012$ GPa^{-1}. The structural transition to the *Pbnm*-phase is accompanied by the unit cell volume change of -7.0%. The evaluated bulk modulus value for the *Pbnm* phase, $B_0 = 295(10)$ GPa is about the same as one found in [20]. The calculated lattice parameters of the *Pbnm* phase at the highest pressure value achieved in the X-ray diffraction experiments $P = 30.5$ GPa, $a = 4.900(9)$, $b = 5.070(9)$, $c = 7.000(15)$ Å, are comparable with those obtained at similar pressures in [20].

3.2 Magnetic structure

Neutron diffraction patterns of $GaFeO_3$, measured for selected pressures and temperatures are shown in Fig. 4. From the Rietveld refinement of ambient pressure data, a degree of the antisite disorder present in the sample was evaluated. In the orthorhombic structure of the $Pc2_1n$ symmetry, the gallium Ga1,2 and iron Fe1,2 atoms are located at positions 4(a) (x, y, z). The obtained values of the coordinates of these atoms at ambient conditions, Ga1 – (0.153(1), 0, 0.171(1)), Ga2 – (0.156(1), 0.317(2), 0.833(3)), Fe1 - (0.162(1), 0.589(3), 0.203(2)) and Fe2 - (0.033(1), 0.813(3), 0.676(3)) are consistent with previous studies [11]. The occupation of Ga2 site by Fe atoms was found to be ~ 0.26, and this is compensated by the same occupation of Ga atoms on Fe2 sites. The Fe atoms located at Ga2 site will be further denoted as Fe3. No antisite disoder in Ga1/Fe1 positions was detected.

Upon cooling below ambient temperature, rapid increase of the intensities of the peaks (200) at $d_{hkl} \approx 4.65$ Å and (101) at $d_{hkl} \approx 6.34$ Å was observed, demonstrating appearance of the long range magnetic order. The analysis of the magnetic contribution to diffraction data suggests the anti-parallel arrangement of Fe1 and Fe2/Fe3 spins, oriented along the c - axis.

For the ideal $GeFeO_3$ crystal, theoretical calculations predict the antiferromagnetic ground state [17]. The values of the Fe ordered magnetic moments located at Fe1 and Fe2 positions, determined from the analysis of the magnetic contribution to neutron diffraction data, are indeed very close, $\mu_{Fe1} \approx \mu_{Fe2} \approx 3.05\ \mu_B$ (Table 1). However, antisite disorder of Fe and Ga atoms leads to a presence of the non-zero magnetic moments at relevant crystallographic position $\mu_{Fe3} \approx 2.5\ \mu_B$ and weak spontaneous magnetization of about 0.07 μ_B per formula unit (Table 1). The obtained values of the ordered magnetic moments and spontaneous magnetization is somewhat less in comparison with previous studies [11, 14, 19], likely due to different sample preparation methods, influencing features of the Ga/Fe site disorder.

The Néel temperature T_N of $GaFeO_3$, calculated from the temperature dependencies of the ordered Fe magnetic moments, increases from 292 to 310 K in the pressure range 0 – 6.2 GPa (fig. 5). The corresponding pressure coefficient $(1/T_N)(dT_N/dP)$ = 0.011(1) GPa^{-1} is comparable with relevant coefficients for the multiferroic relaxor $PbFe_{0.5}Nb_{0.5}O_3$ (0.016 GPa^{-1}) and ferrites $NdFeO_3$ (0.016 GPa^{-1}) and $LuFeO_3$, (0.014 GPa^{-1}) [30, 31]. The T_N value at ambient pressure is close to one found for the high quality single crystal $GaFeO_3$ [19]. The calculated absolute value of the spontaneous magnetization at 10 K exhibits a tendency towards increase by about 50 % in the pressure range 0 – 6.2 GPa (Fig. 5).

3.3 Raman spectroscopy

In $GaFeO_3$ theoretical calculations predict the existence of 120 vibrational modes for the $Pc2_1n$ space group, 117 of which are Raman active modes [14]. In the present study we have identified 22 distinct Raman peaks in the spectral range 150 - 900 cm^{-1} at ambient pressure, located at frequencies 173, 198, 219, 238, 258, 281, 290, 304, 345, 358, 374, 390, 437, 467, 513, 573, 604, 639, 663, 691, 723 and 746 cm^{-1}. For comparison, Mukherjee *at al* [19] revealed 32 phonon modes in the frequency range 90 - 900 cm^{-1} for high quality single crystal of $GaFeO_3$, and positions of 22 of these modes are close to those found in our study.

The Raman spectra of $GaFeO_3$, containing a combination of tetrahedral $(Ga,Fe)O_4$ and octahedral $(Ga,Fe)O_4$ structural units can be compared with those of cubic magnetite Fe_3O_4 [32, 33] and rhombohedral hematite Fe_2O_3 [34] and ortoferrites [35, 36, 37], which Raman active modes in the discussed frequencies range are generally associated with vibrations of either FeO_4 tetrahedra or FeO_6 octahedra, respectively. Such a comparison allows to assign the high frequency modes in the 650 – 750 cm^{-1} to symmetric stretching vibrations of $(Ga,Fe)O_4$ tetrahedra, the modes in the range 600 – 650 cm^{-1} to symmetric stretching vibrations of $(Ga,Fe)O_6$ octahedra, the modes in the range 500-590 cm^{-1} to asymmetric stretching of $(Ga,Fe)O_4$ tetrahedra and $(Ga,Fe)O_6$ octahedra. The modes in the range 400-490 cm^{-1} likely correspond to bending vibrations and those in the range 150 – 390 cm^{-1} to rotational vibrations of $(Ga,Fe)O_4$ tetrahedra and $(Ga,Fe)O_6$ octahedra and translational vibrations.

For the analysis of pressure effects, eleven appropriately resolved modes were chosen and labeled as m1 … m11 (Fig. 6, Table 2). In the pressure range below 21 GPa, corresponding to the orthorhombic $Pc2_1n$ – phase, the frequencies of these modes increase nearly linearly (Fig. 7). The m9, m10 and m11 modes, have similar pressure coefficients ($k_{mi} = \{1/v_{mi0}\}\cdot dv_{mi}/dP$) 0.0039-0.0046 GPa^{-1} and Grüneisen parameters ($\gamma_{mi} = -\partial(\ln v_i)/\partial \ln V$) 0.79-0.93 (Table 2). These values of

the Grüneisen parameters are comparable with ones found for the stretching modes of the FeO_4 tetrahedra in magnetite Fe_3O_4 [38] and ferrite spinels $MgFe_2O_4$ and $ZnFe_2O_4$ [39, 40], supporting the above modes assignment. The pressure coefficient and Grüneisen parameter of the m8 mode, associated with the symmetric stretching of the $(Fe,Ge)O_6$ octahedra, are noticeably larger, 0.0062 GPa^{-1} and 1.25, respectively. These values are similar to ones found for the stretching mode of FeO_6 octahedra in Fe_2O_3 [34]. The frequencies of the stretching modes are mediated by the (Ga,Fe)-O bonds and the above difference in the pressure coefficients implies larger compressibility of the octahedral $(Ga,Fe)O_6$ units in comparison with the tetrahedral $(Ga,Fe)O_4$ ones. The comparison of pressure coefficients and Grüneisen parameters of the modes in bending region (Table 2) allows to associate the m6 mode with the vibrations of $(Ga,Fe)O_6$ octahedra and m7 one with the vibrations of the $(Ga,Fe)O_4$ tetrahedra.

The m1 – m3 modes have the lowest pressure coefficients 0.0019 – 0.0031 GPa^{-1} and Grüneisen parameters 0.38-0.63, which are about twice smaller in comparison with those found for the translational modes in Fe_3O_4 [38] and $ZnFe_2O_4$ [40]. The values of the pressure coefficients and Grüneisen parameters for the m1-m3 modes are comparable with those of rotational modes in lead ferroniobate $PbFe_{0.5}Nb_{0.5}O_3$ [30]. Therefore these modes may correspond to the rotational oxygen vibrations in octahedral and tetrahedral structural units.

In the vicinity of the structural phase transition to the orthorhombic *Pbnm* phase, starting at 21 GPa, noticeable changes in Raman spectra occur. A merging of the m6 and m7 modes, and changes in the intensity of several Raman modes were detected (Figs. 6 and 7, Table 2). The main structural units of the *Pbnm* phase are $(Ga,Fe)O_6$ octahedra, so the Raman modes associated with the $(Ga,Fe)O_4$ tetrahedra in the initial $Pc2_1n$ should be gradually suppressed during the phase transition. The pressure coefficients and Grüneisen parameters of the stretching and bending modes with frequencies values above 400 cm^{-1} are reduced significantly at pressures above 21 GPa (Table 2, Fig. 7), while relevant values of lower frequency modes remain nearly the same over the whole studied pressure range.

Due to the broad pressure range of the phase coexistence, it was difficult to distinguish unambiguously particular modes corresponding to the *Pbnm* phase. In the recent structural study of $GaFeO_3$ [20], the pure *Pbnm* phase was observed for pressures above 42 GPa. The highest pressure, achieved in the present study, was 41.8 GPa and it is reasonable to suggest that Raman spectrum measured for this value (Fig. 6) corresponds to the prevailing *Pbnm* phase. It contains seven resolved peaks at ~ 247, 326, 344, 369, 522, 566, 788 cm^{-1}. The group theory predicts 24 Raman-active phonon modes for the *Pnma* symmetry, $\Gamma_{Ram} = 7A_g + 7B_{1g} + 5B_{2g} + 5B_{3g}$ [41]. According to previous studies of isostructural orthoferrites [35, 36, 42, 43], the observed modes can be assigned to B_{2g} (788 cm^{-1}) and A_g (566 cm^{-1}) stretching modes, A_g (369 cm^{-1}) and B_{1g}

(522 and 344 cm^{-1}) bending modes, B_{1g} (326 cm^{-1}) and A_g (247 cm^{-1}) rotation modes of $(Ga,Fe)O_6$ octahedra. Further studies in the extended pressure range are necessary to evaluate pressure coefficients and Grüneisen partameters of the Raman active modes of the pressure induced *Pbnm* phase.

4. Conclusions

The present results demonstrate that at elevated pressures the magnetic ordering in the polar orthorhombic $Pc2_1n$ phase of $GaFeO_3$ occurs above room temperature and the Néel temperature raises with the positive pressure coefficient of 0.011 GPa^{-1}. The spontaneous magnetization calculated from the ordered Fe magnetic moments at T = 10 K exhibits a tendency towards increase by about 50 % in the 0 – 6.2 GPa pressure range. Analysis of the pressure coefficients and Grüneisen parameters of the Raman modes implies the larger compressibility of the tetrahedral $(Ga,Fe)O_4$ structural units in comparison with the octahedral $(Ga,Fe)O_6$ ones in the $Pc2_1n$ phase. At pressures above 21 GPa, a gradual phase transition into the non-polar orthorhombic *Pbnm* phase occurs. It modifies significantly the Raman spectra, resulting in suppression of the vibrational modes involving tetrahedral $(Ga,Fe)O_4$ structural units and anomalies in pressure dependences of the high frequency modes associated with vibrations of the $(Ga,Fe)O_6$ oxygen octahedra.

Acknowledgements

The work has been supported by the RFBR grant 15-02-03248-a.

References

[1] G.A. Smolenskii and I.E. Chupis, Sov. Phys. Usp. 25 (1982) 475.

[2] M. Fiebig, J. Phys. D 38 (2005) R123.

[3] T. Kimura, T. Goto, H. Shintani, K. Ishizaka, T. Arima, and Y. Tokura, Nature 426 (2003) 55.

[4] S.-W. Cheong and M. Mostovoy, Nature Mater. 6 (2007) 13.

[5] M. Kenzelmann, G. Lawes, A.B. Harris, G. Gasparovic, C. Broholm, A.P. Ramirez, G.A. Jorge, M. Jaime, S. Park, Q. Huang, A.Ya. Shapiro, and L.A. Demianets, Phys. Rev. Lett. 98 (2007) 267205.

[6] Ogawa Y., Kaneko Y., He J.P., Yu X.Z., Arima T. and Tokura Y., Phys. Rev. Lett. 92 (2004) 047401.

[7] J.H. Jung, M. Matsubara, T. Arima, J.P. He, Y. Kaneko and Y. Tokura Phys. Rev. Lett. 93 (2004) 037403.

[8] J.P. Remeika, J. Appl. Phys. 31 (1960) 263S.

[9] G.T. Rado, Phys. Rev. Lett. 13 (1964) 335.

[10] Z.H. Sun, B.L. Cheng, S. Dai, L.Z. Cao, Y.L. Zhou, K.J. Jin, Z.H. Chen and G.Z. Yang, J. Phys. D: Appl. Phys. 39 (2006) 2481.

[11] T. Arima, D. Higashiyama, Y. Kaneko, J.P. He, T. Goto, S. Miyasaka, T. Kimura, K. Oikawa, T. Kamiyama, R. Kumai, and Y. Tokura, Phys. Rev. B 70 (2004) 064426.

[12] S.K. Mishra, R. Mittal, Ripandeep Singh, S.L. Chaplot, M. Zbiri, T. Hansenk, and H. Schober, J. Appl. Phys. 113 (2013) 174102.

[13] S.C. Abrahams, J.M. Reddy, and J.L. Bernstein, The Journal of Chemical Physics 42 (1965) 3957.

[14] Kavita Sharma, V. Raghavendra Reddy, Deepti Kothari, Ajay Gupta, A. Banerjee and V.G. Sathe, J. Phys.: Condens. Matter 22 (2010) 146005.

[15] R. Saha, A. Shireen, A.K. Bera, S.N. Shirodkar , Y. Sundarayya, N. Kalarikkal, S.M. Yusuf, U.V. Waghmare, A. Sundaresan, C.N.R. Rao, J. Solid State Chem. 184 (2011) 494.

[16] R.B. Frankel, N.A. Blum, S. Foner, A.J. Freeman, M. Schieber, Phys. Rev. Lett. 15 (1965) 958.

[17] Myung Joon Han, Taisuke Ozaki, and Jaejun Yu, Phys. Rev. B 75 (2007) 060404(R).

[18] Mayanak Kumar Gupta, Ranjan Mittal, Mohamed Zbiri, Ripandeep Singh, Stephane Rols, Helmut Schober, and Samrath Lal Chaplo, Phys. Rev. B 90 (2014) 134304.

[19] Somdutta Mukherjee, Ashish Garg and Rajeev Gupta, J. Phys.: Condens. Matter 23 (2011) 445403.

[20] R. Arielly, W.M. Xu, E. Greenberg, G.Kh. Rozenberg, M.P. Pasternak, G. Garbarino, S. Clark, and R. Jeanloz, Phys. Rev. B 84 (2011) 094109.

[21] Gregory Kh. Rozenberg, Weiming Xu and Moshe P. Pasternak, Z. Kristallogr. 229(3) (2014) 210.

[22] H.-P. Liermann, W. Morgenroth, A. Ehnes, A. BerghaËuser, B. Winkler, H. Franz, and E. Weckert, J. Phys. Conf. Ser. 215 (2010) 012029.

[23] A.P. Hammersley, S.O. Svensson, M. Hanfland, A.N. Fitch, and D. Hausermann, High Press. Res. 14 (1996) 235.

[24] V.L. Aksenov, A.M. Balagurov, V.P. Glazkov, D.P. Kozlenko, I.V. Naumov, B.N. Savenko, D.V. Sheptyakov, V.A. Somenkov, A.P. Bulkin, V.A. Kudryashev, and V.A. Trounov, Physica B 265 (1999) 258.

[25] V.P. Glazkov and I.N. Goncharenko, Fiz. I Technika Vysokih Davlenij 1 (1991) 56 (in Russian).

[26] H.K. Mao, P.M. Bell, J.W. Shaner, and D.J. Steinberg, J. Appl. Phys. 49 (1978) 3276.

[27] J. Rodrıгguez-Carvajal, Physica B 192 (1993) 55.

[28] N.A. Dubrovinskaia and L.S. Dubrovinsky, Rev. Sci. Instrum. 74 (2003) 3433.

[29] F.J. Birch, J. Geophys. Res. 91 (1986) 4949.

[30] D.P. Kozlenko, S.E. Kichanov, E.V. Lukin, N.T. Dang, L.S. Dubrovinsky, H.-P. Liermann, W. Morgenroth, A.A. Kamynin, S.A. Gridnev, and B.N. Savenko, Phys. Res. B 89 (2014) 174107.

[31] A.G. Gavriliuk, G.N. Stepanov, I.S. Lyubutin, A.S. Stepin, I.A. Trojan, and V.A. Sidorov, Hyperfine Interact. 126 (2000) 305.

[32] Olga N. Shebanova and Peter Lazor, J. Solid State Chem. 174 (2003) 424.

[33] J. Larry Verble, Phys. Rev. B 9 (1974) 5236.

[34] Sang-Heon Shim and Thomas S. Duffy, American Mineralogist 87 (2001) 318.

[35] Shankar Ghosh, N. Kamaraju, M. Seto, A. Fujimori, Y. Takeda, S. Ishiwata, S. Kawasaki, M. Azuma, M. Takano, and A. K. Sood, Phys. Rev. B 71 (2005) 245110.

[36] G.Kh. Rozenberg, M.P. Pasternak, W.M. Xu ,L.S. Dubrovinsky, S. Carlson and R.D. Taylor, Europhys. Lett. 71 (2) (2005) 228.

[37] H.C. Gupta, Manoj Kumar Singh and L.M. Tiwari, J. Raman Spectrosc. 33 (2002) 67.

[38] Olga N. Shebanova and Peter Lazor, J. Chem. Phys. 119 (2003) 6100.

[39] Zhongwu Wanga, P. Lazorb, S.K. Saxenaa, Hugh St. C. O'Neill, Mater. Res. Bull. 37 (2002) 1589.

[40] Zhongwu Wanga, David Schiferla, Yusheng Zhaoa, H.St. C. O'Neil, J. Phys. and Chem. of Solids 64 (2003) 2517.

[41] M.N. Iliev, and M.V. Abrashev, J. Raman Spectrosc. 32 (2001) 805.

[42] S. Venugopalan, Mitra Dutta, A. K. Ramdas, J. P. Remeika, Phys. Rev. B 31 (1985) 1490.

[43] Manoj K.Singh, Hyun M. Jang, H.C. Gupta and Ram S. Katiyar, J. Raman Spectrosc. 39 (2008) 842.

Table 1.

Calculated ordered magnetic moments μ for Fe1, Fe2 and Fe3 sites in the orthorhombic $Pc2_1n$ phase of $GaFeO_3$ and net magnetization $\mu_{f.u.}$ per formula unit at T = 10 K and selected pressures.

P, GPa	0	2.5	6.2
μ(Fe1), μ_B	-3.070(10)	-3.0(1)	-3.0(1)
μ(Fe2), μ_B	3.057(9)	3.0(1)	2.9(1)
μ(Fe3), μ_B	2.498(9)	2.3(1)	2.4(1)
$\mu_{f.u.}$, μ_B /f.u.	-0.0798(3)	-0.09(3)	-0.12(3)

Table 2.

Pressure coefficients $k_{mi} = \{1/v_{mi0}\}\cdot dv_{mi}/dP$ and Grüneisen parameters $\gamma_{mi} = -\partial(\ln v_i)/\partial \ln V$ of Raman modes in $GaFeO_3$ at pressure ranges below and above the structural transition pressure $P \sim 21$ GPa.

Raman mode, m_i	Frequency, cm^{-1}	k_{vmi} (GPa^{-1})	γ_{mi}
m1	238	0.0019	0.38
m2	304	0.0038	0.77
m3	358	0.0031	0.63
m4	374	0.0048	0.98
m5	390	0.0054	1.10
m6	437	0.0069 (P < 21 GPa) 0.0017 (P > 21 GPa)	1.42 0.34
m7	467	0.0039 (P < 21 GPa) 0.0017 (P > 21 GPa)	0.79 0.34
m8	604	0.0062 (P < 21 GPa) 0.0019 (P > 21 GPa)	1.25 0.39
m9	691	0.0046 (P < 21 GPa) 0.0008 (P > 21 GPa)	0.93 0.16
m10	722	0.0039 (P < 21 GPa) 0.0006 (P > 21 GPa)	0.79 0.13
m11	746	0.0042 (P < 21 GPa) 0.0013 (P > 21 GPa)	0.85 0.26

Fig. 1. (Color online) Left panel: X-ray diffraction patterns of $GaFeO_3$ measured at selected pressures and ambient temperature and refined by the Rietveld method. Experimental points, calculated profiles and difference curve (for P = 0 GPa) are shown. Tick marks at the bottom and top represent the calculated positions of diffraction peaks for the $Pc2_1n$ orthorhombic phase (at P = 0 GPa) and *Pbnm* orthorhombic phase (at P = 30.5 GPa), respectively. In the right panel a more detailed view of the patterns measured at pressures P = 14.5 (top) and 30.5 GPa (bottom) is given, including difference curves. Tick marks represent the calculated positions of diffraction peaks for the $Pc2_1n$ orthorhombic phase (P = 14.5 GPa) and for coexisting orthorhombic phases $Pc2_1n$ (upper row) and *Pbnm* (lower row) for P = 30.5 GPa.

Fig. 2. (Color online) Schematic crystal structure of ambient pressure $Pc2_1n$ (left) and high pressure *Pbnm* (right) orthorhombic phases of $GaFeO_3$.

Fig. 3. (Color online) Lattice parameters and unit cell volume of the $Pc2_1n$ orthorhombic phase of $GaFeO_3$ as functions of pressure and their interpolation based on the Birch-Murnaghan equation of state. The pressure dependence of the unit cell volume for the pressure-induced *Pbnm* phase is also shown.

Fig. 4. (Color online) Neutron diffraction patterns of $GaFeO_3$, measured at 290 K and 10 K (inserts) at pressures 0 GPa (top pattern) and 2.5 GPa (lower pattern), processed by the Rietveld method. The experimental points, calculated profiles and differences curves are shown. The ticks below represent positions of structural and magnetic diffraction peaks. Peaks with ferrimagnetic contribution are marked as Ferrimag (inserts). In patterns measured at P = 2.5 GPa external peaks from the pressure cell are labeled by mark "S" (they were considered in the fitting process).

Fig. 5. (Color online) (a) Temperature dependences of the ordered Fe magnetic moments in Fe1,2,3 crystallographic sites of the $Pc2_1n$ orthorhombic phase of $GaFeO_3$ at selected pressures, normalized to the values obtained at T = 10 K. Solid and dashed lines represent interpolations by functions $\mu = \mu_0(1-(T/T_N)^{\alpha})^{\beta}$. (b) Pressure dependence of the Néel temperature and its linear interpolation. (c) Pressure dependence of the absolute value of the spontaneous magnetization and its linear interpolation.

Fig. 6. (Color online) Left panel: Raman spectra of $GaFeO_3$ at selected pressures and ambient temperature. Right panel: Pressure dependent Raman spectra of $GaFeO_3$ at selected pressures in the Raman shift range 550 - 900 cm^{-1}. Spectra were fitted with a combination of the Pearson-VII functions. The most intense modes discussed in the text are marked as m8-m11.

Fig. 7. (Color online) Pressure dependencies of the m1-m11 modes frequencies and their linear interpolation. The error bars are within the symbol size. Dashed lines denote the pressure P = 21 GPa corresponding to the $Pc2_1n$ - *Pbnm* structural phase transition.

Fig.1.

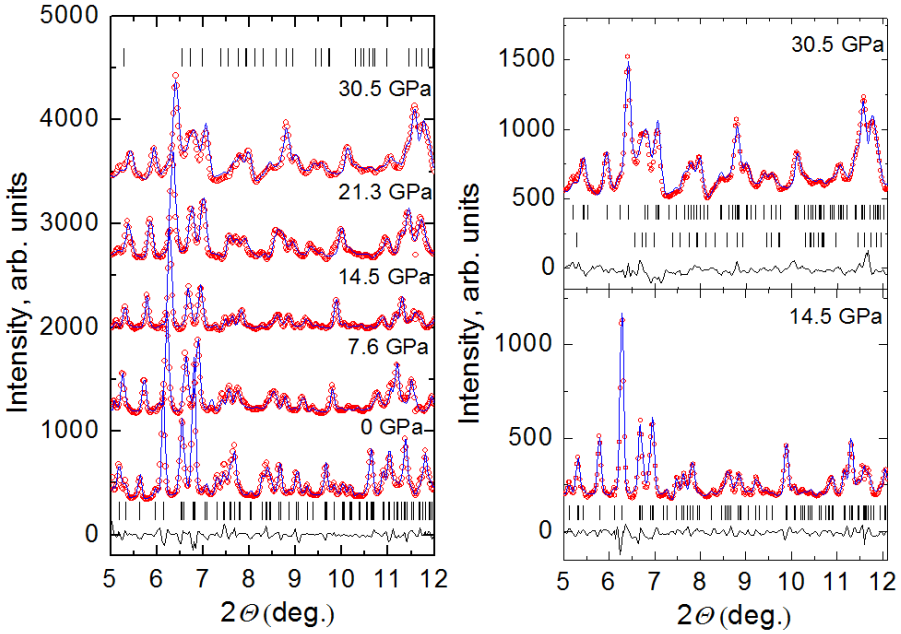

Fig. 2.

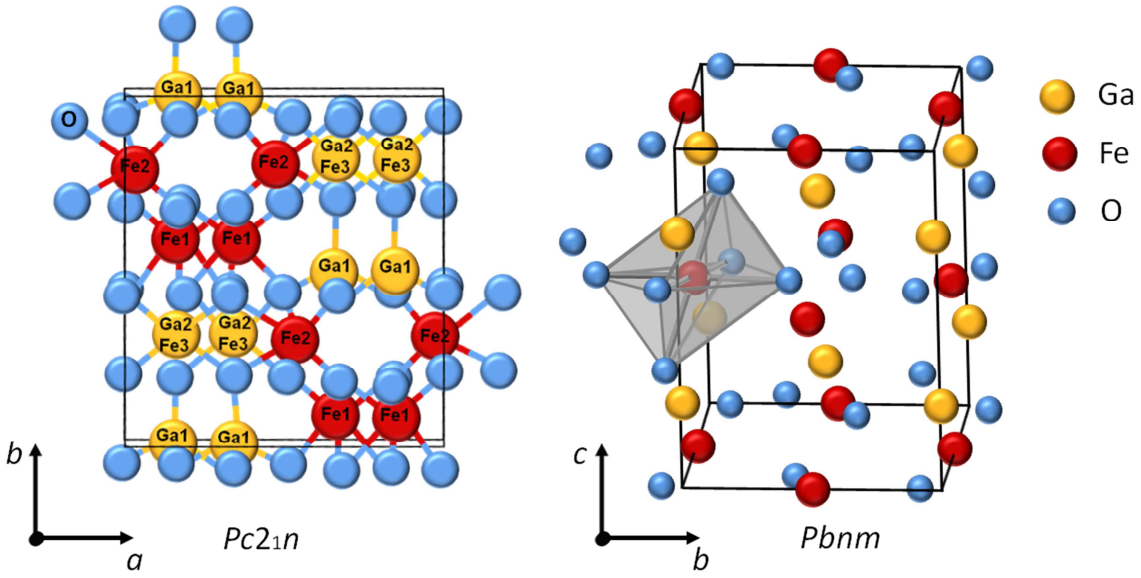

Fig. 3.

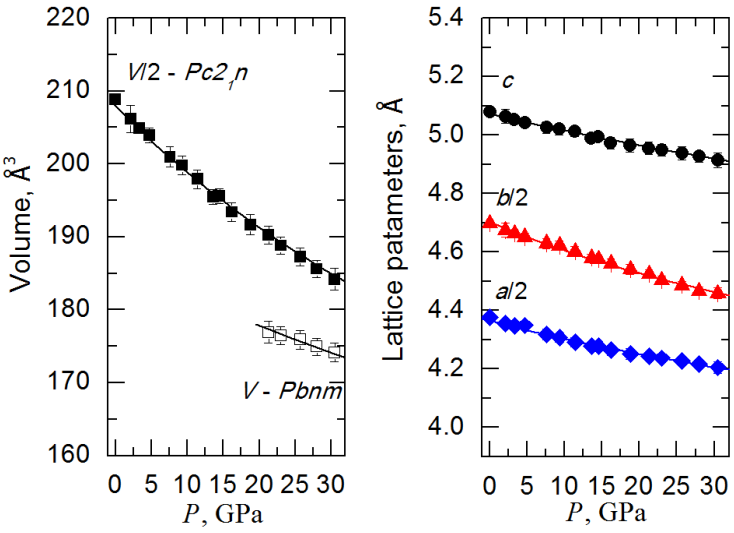

Fig. 4.

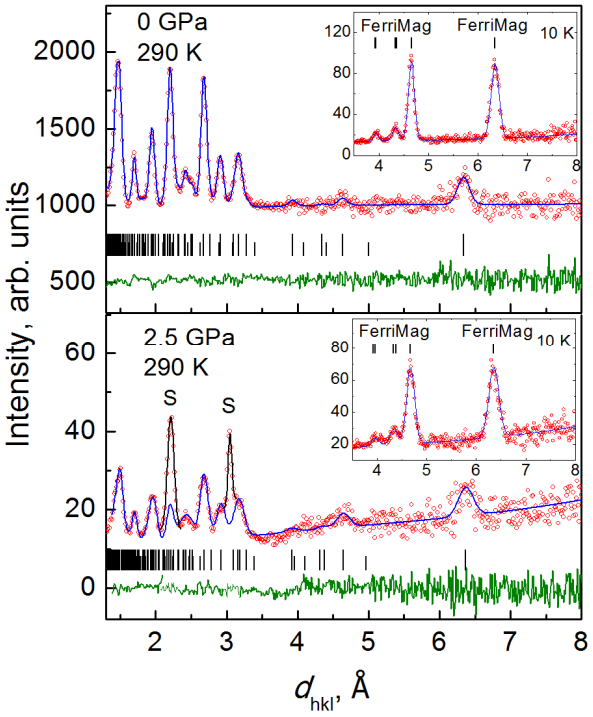

Fig. 5.

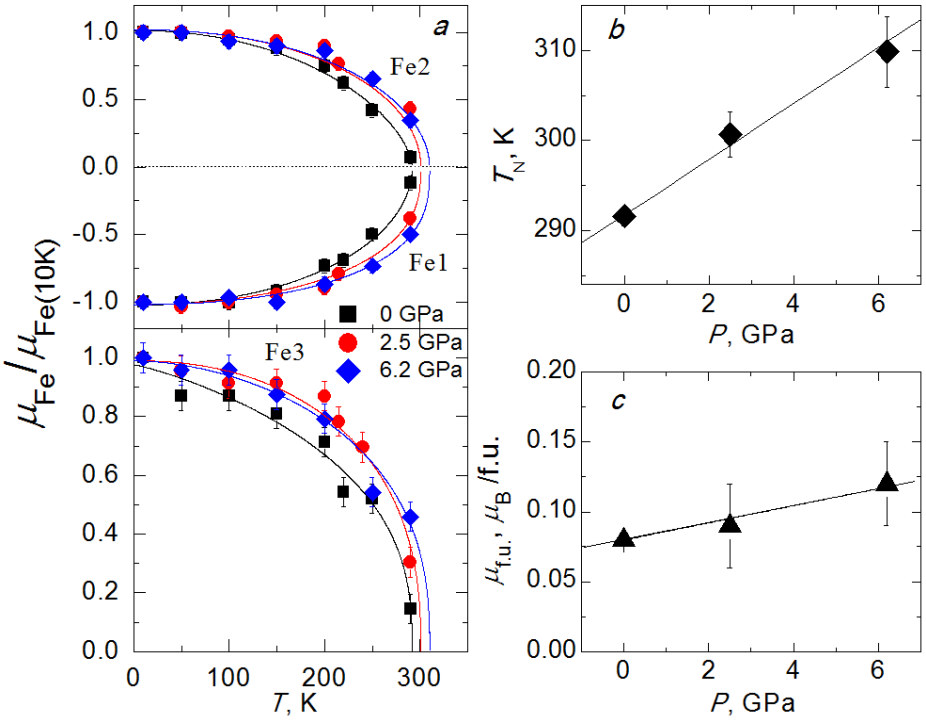

Fig. 6.

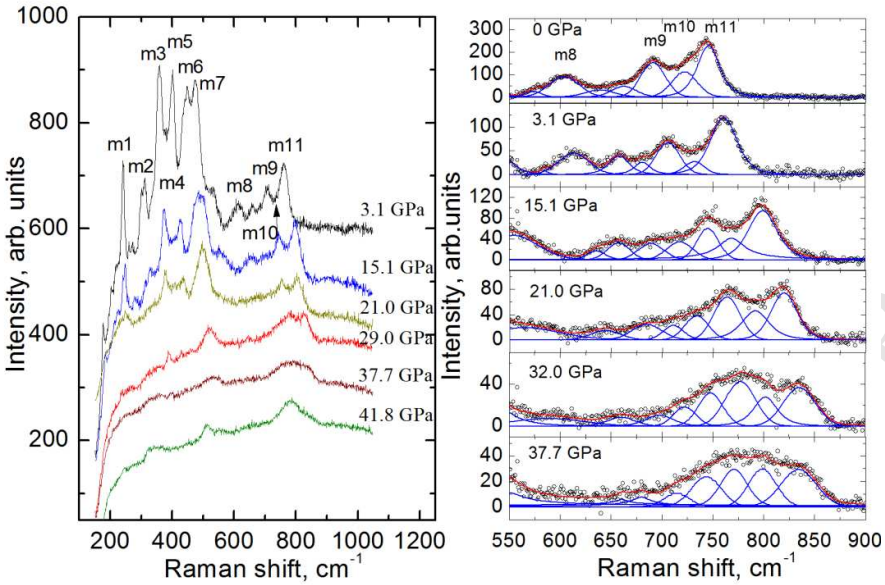

Fig. 7.

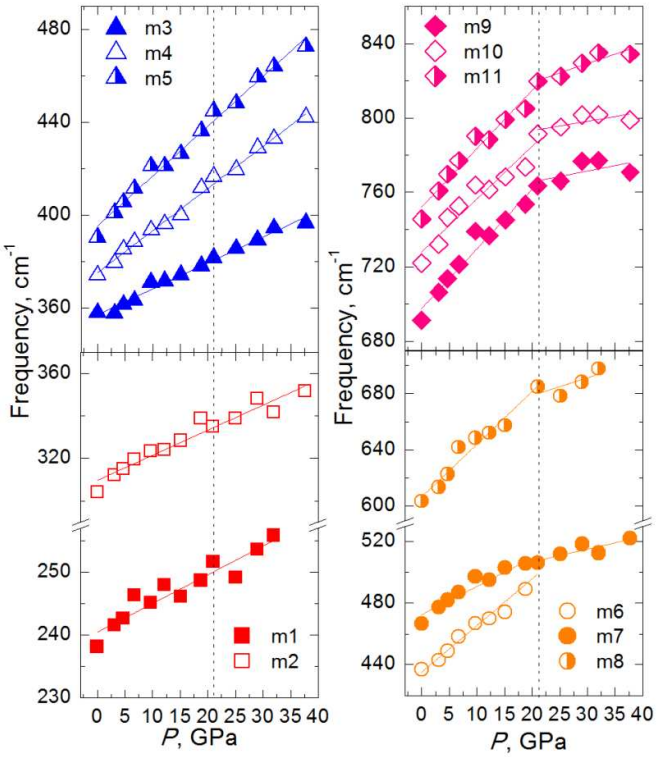

Highlights:

1. Magnetic structure of $GaFeO_3$ is changed under pressure

2. The Néel temperature of $GaFeO_3$ is close to room temperature

3. The Néel temperature of $GaFeO_3$ raises under pressure

4. The spontaneous magnetization exhibits a tendency towards increase under pressure in $GaFeO_3$

5. Application of high pressure leads to changes in Raman spectra of $GaFeO_3$ at structural phase transition